Electronic structure of multiferroic $BiFeO_3$ and related compounds: Electron energy loss spectroscopy and density functional study

Ragnhild Sæterli,[1] Sverre Magnus Selbach,[2] Ponniah Ravindran,[3] Tor Grande,[2] and Randi Holmestad[1,*]
[1]*Department of Physics, Norwegian University of Science and Technology (NTNU), 7491 Trondheim, Norway*
[2]*Department of Materials Science and Engineering, Norwegian University of Science and Technology (NTNU), 7491 Trondheim, Norway*
[3]*Department of Chemistry, University of Oslo, P.O. Box 1033, Blindern, N-0315 Oslo, Norway*
(Received 26 February 2010; revised manuscript received 7 May 2010; published 6 August 2010)

The electronic structure of complex oxides is important for the understanding of their functional properties. In this paper, the electronic structures of the multiferroic perovskite bismuth ferrite ($BiFeO_3$) and the related isostructural compounds $Bi_{0.9}La_{0.1}FeO_3$ and $BiFe_{0.7}Mn_{0.3}O_3$ are investigated through experiments and modeling. Using electron energy loss spectroscopy the oxygen *K* edge, i.e., the unoccupied O *p* density of states, is probed. As these states participate in covalent bonding with both Bi and Fe states, insight into the bonding in the materials is obtained. By substituting on both cation sites, it is possible to connect features in the spectrum to chemical bonds to the cations. We compare the experimental results of substituted and unsubstituted $BiFeO_3$ and apply a multiple-scattering approach as well as density functional theory to interpret the differences in terms of changes in electronic structure and density of states. Specifically, we show that although mainly ionic, both Bi-O and Fe-O bonds have some covalent character, and that Mn substitution on Fe sites is found to alter the Bi-O bonds and reduce the anisotropy of the system. Upon introduction of La on Bi sites, the covalent character of the material is reduced and the ionic interaction increases as the La-O bond is higher in energy and mediated through other cation orbitals (La *d* orbitals) than the Bi-O bond (Bi *p* orbitals). Also, La substitution is found to influence the Fe electronic structure, showing that the *A* and *B* site cations are more coupled than commonly recognized. Thus, we use the electronic structure to confirm that *B* site cation substitution can influence the ferroelectricity, which is usually almost exclusively attributed to *A* site cation anisotropy.

DOI: 10.1103/PhysRevB.82.064102 PACS number(s): 79.20.Uv, 71.15.Mb, 75.85.+t, 71.20.Nr

I. INTRODUCTION

The past few years have seen a huge interest in bismuth ferrite ($BiFeO_3$, BFO).[1–3] This is largely due to its unique combination of ferroic properties that extends up to and above room temperature, as it is antiferromagnetic with a Néel temperature of 370 °C and ferroelectric with a Curie temperature of about 825 °C. When these properties are coupled through the magnetoelectric effect, a range of application possibilities opens up including memory devices, sensors and spintronics.[4]

BFO has a distorted perovskite (ABO_3) structure, with a room-temperature ground state belonging to the rhombohedral space group *R*3*c*. In the hexagonal setting, the unit-cell parameters are a_h=5.58 Å and c_h=13.87 Å,[5] corresponding to a rhombohedral angle of 59.35°. Compared to an ideal (cubic) perovskite structure, oxygen octahedra are antiferrodistortively rotated by 13.8° about the pseudocubic [111] axis, and Fe and Bi atoms are both shifted along the pseudocubic [111] direction by 0.13 Å and 0.54 Å, respectively, giving four different O-O bond lengths. The large displacement of Bi is consistent with the idea of a stereochemically active lone pair of electrons that is found to push the Bi atoms in the pseudocubic [111] direction and thus be the cause of ferroelectricity in BFO.[6] As in other perovskites, the bonding in BFO is mostly ionic with Bi and Fe in a (nominally) 3+ state and O in 2−. These valences are altered by the introduction of a covalent contribution to the bonding, and it is this covalency, however small, that is responsible for the ferroic properties that make BFO interesting.

Recently, scientific effort has been directed at enhancing the ferroic properties of BFO by substitution on Bi (*A*) and Fe (*B*) sites,[7–9] however most studies have been focused on thin films rather than bulk ceramics. In bulk $Bi_{1-x}La_xFeO_3$, La substitution has been reported to enhance ferroelectric properties,[10–13] although most of this enhancement is believed to arise from a reduction in secondary phases, oxygen vacancies and valence fluctuations of Fe (Ref. 11) that increase leakage currents and thereby make polarization measurements challenging. Thus, the influence of La substitution on bulk, stoichiometric BFO remains largely unknown. The same thing can be said about the pure bulk (single-crystalline and defect-free) electronic properties when Mn is substituting Fe in $BiFe_{1-x}Mn_xO_3$.[14,15]

While there seems to be a consensus that Mn- and La-substituted $BiFeO_3$ remains *R*3*c* for $x_{Mn} \leq 0.3$ (Refs. 16–18) and $x_{La} \leq 0.1$ for $x_{La} > 0.1$ the structure is under debate.[11,19–22] We have therefore chosen to focus our attention on the isostructural, however less distorted, and still ferroelectric and antiferromagnetic compounds with La and Mn contents of x_{La}=0.1 and x_{Mn}=0.3, respectively, while other amounts of substitution provide interesting subjects for further studies on both structural and electronic properties.

Recently, some work has been published on the electronic structure of BFO and its substituted relatives, mostly on theoretical grounds using density functional theory (DFT) (Refs. 1, 6, and 20) in addition to a few experimental x-ray absorption spectroscopy (XAS) studies.[23–25] Most transmission electron microscopy (TEM) studies related to BFO have focused on structural characterization, mostly on nanopowders[26–28] or thin films,[29–33] rather than electronic properties.

Here, we describe the energy loss near-edge structure (ELNES) of BFO, $Bi_{0.9}La_{0.1}FeO_3$ (BLFO), and

$BiFe_{0.7}Mn_{0.3}O_3$ (BFMO), focusing on the changes to the oxygen *K* edge. To a first approximation, this O *K* edge stems from transitions from the O 1*s* orbital to unoccupied O states of *p* symmetry. For the O *K* edge in O^{2-} materials, any fine structure present is simply a result of (partial) covalent bonding as all 2*p* states are occupied and no available *p* states are found just above E_F in the purely ionic case. In perovskites, the O 2*p* states are known to form covalent bonds with the B atom *d* states[34] and in some cases also to *A* atom states,[35] pushing some of the otherwise occupied O *p* states above E_F. Hence, the O *K* edge is very sensitive to variations in bonding, covalency, and, with that, ferroic properties.

We interpret the experimental O *K* edge of BFO in terms of local density of states (DOS) from real-space multiple scattering (RSMS) as well as DFT calculations, and employ this interpretation to shed light on the changes in electronic structure as Fe and Bi is substituted by Mn and La, respectively.

II. EXPERIMENTAL SECTION

A. Materials

BFO, BFMO, and BLFO powder samples were prepared by solid-state reaction between stoichiometric amounts of dried Bi_2O_3 (Aldrich >99.9%), Fe_2O_3 (Sigma-Aldrich 99.98%), La_2O_3 (Merck >99%), and Mn_2O_3 [prepared from Riedel-de Haën $Mn(CH_3COO)_2 \cdot 4H_2O$ >99.5% by annealing in air at 700 °C for 8 h]. Pellets of stoichiometric binary oxide mixtures were immersed in sacrificial powder, in order to eliminate possible evaporation of Bi_2O_3, and fired once for 10 min at 900 °C before quenching in air. The temperature-time program was chosen to minimize the amounts of residual secondary phases.[16] The BFMO sample was further annealed at 850 °C for 30 min in flowing 5.0 N_2 and cooled to ambient temperature at 400 °C h^{-1} to avoid excess oxygen, as described previously.[17,36]

B. Transmission electron microscopy and x-ray diffraction

TEM specimens were prepared by crushing particles in ethanol which were left to dry on a TEM copper grid with amorphous holey carbon film. X-ray diffraction (XRD) as well as electron diffraction and energy dispersive x-ray spectroscopy were used to check structure and composition of the produced batch and individual particles used for energy loss analysis.

XRD patterns were collected from 20° to 96° 2θ with a total acquisition time of 4.5 h per sample with a θ-2θ Bruker AXS Focus diffractometer with Cu $K\alpha$ radiation and a Lynx-Eye position sensitive detector. Rietveld refinements were carried out with the software TOPAS R (Bruker AXS), using the space group *R*3*c* (161) in the hexagonal setting. Differential thermal analysis (DTA) was done with a Netzsch STA 449 C Jupiter in synthetic air with 10 °C min^{-1} heating rate.

C. Energy loss near-edge structure ELNES

Electron energy loss spectroscopy (EELS) and ELNES are techniques much used in the study of electronic structure of materials.[37,38] By mapping out the energy loss of the electrons that have passed through a thin (<100 nm) TEM specimen, information on the unoccupied density of states can be obtained through core loss interactions. As beam electrons excite specimen electrons, they lose an amount of energy depending on (i) the energy levels of the excited atoms and (ii), what is employed in ELNES, the DOS above the Fermi energy. The allowed excitation processes are (usually) governed by the dipole selection rule, predicting that only transitions between states with a difference in angular momentum Δl of ± 1 are allowed. Furthermore, as initial and final states are restricted to the same atom, ELNES measures the site- and symmetry-specific DOSs.[37] However, as with the related technique x-ray absorption near-edge spectroscopy (XANES), the DOS is influenced by the presence of a core hole and one is thus strictly speaking not measuring the ground states. The influence of the core hole can vary from material to material (see, e.g., the work of van Benthem *et al.*[39] on $SrTiO_3$ and their discussion), however the differences are usually assumed small and comparison to ground-state calculations like DFT is still useful.

Control of the experimental parameters is vital to any quantitative or qualitative EELS work. The ELNES spectra in this study were all taken at a JEOL 2010F with a Gatan imaging filter attached, operated at 200 kV in convergent beam diffraction mode with beam convergence and collection angles of 4–5 mrad. Convergent beam mode was chosen to ensure consistency in the results, as a parallel beam was found to give too much variation between the acquired spectra and thus inconsistent results, probably due to sample thickness changes within the examined sample area. For the same reason diffraction mode was used, as it is well known that imaging mode is more prone to erroneous interpretation.[38] The energy resolution of all spectra is comparable and about 1 eV, measured as the full width at half maximum of the zero-loss peak. All spectra were recorded on a dark current subtracted and gain corrected CCD. The background in all spectra has been subtracted by fitting an exponentially decaying function to an energy window of 10 eV just before the edge onset. To avoid multiple inelastic scattering, spectra were acquired from areas of a thickness of 0.2–0.5 mean-free paths. Still, spectra were deconvoluted to ensure a single-scattering distribution, using the Fourier-ratio method in DIGITALMICROGRAPH and a low-loss spectrum from the same area of the specimen taken shortly before or after the core-loss spectrum. A sum of several spectra from each material was used for better counting statistics, and care was taken to avoid strong channeling conditions.[40] No attempts have been made to measure the absolute edge onset of the materials, thus the onsets have been shifted to match those of the calculated spectra.

D. Calculations

We examine the near-edge structure by comparing the experimental edges to both DFT and RSMS calculations. Though formally equivalent, DFT calculations are performed in reciprocal space and can thus deal with large periodic structures while RSMS calculations[41,42] are performed on a

smaller real-space cluster of atoms that can easier accommodate nonperiodic features such as core holes, vacancies, doping, or defects. These two calculation approaches are related to one of the two different schemes of interpreting ELNES and XANES; the density of states and the multiple-scattering interpretation: near the edge onset, the scattered electrons do not have enough energy to escape the excited atom and will be trapped in the more localized unoccupied states, with a probability depending on the density of these states. The energy loss intensity will thus be a measure of the local unoccupied DOS of the correct symmetry, however modified by an energy dependent but slowly varying matrix element. Further above the edge onset, the electrons lose enough energy to probe the more featureless, free-electronlike states, but are also more prone to interference effects as they are elastically scattered by the surrounding atoms. This gives rise to perturbations of the local potential, visible as intensity variations in the high-energy loss area.[37] These two perspectives come together as the near-edge features can be interpreted as single-scattering events due to potential perturbations from the nearest-neighbor atoms, thus the preferred approach depends on the desired information.

First-principles DFT calculations were performed using the Vienna *ab initio* simulation package (VASP) (Ref. 43) within the projector augmented wave method[44] as implemented by Kresse and Joubert.[45] The forces on the atoms were calculated using the Hellmann-Feynman theorem and they are used to perform a conjugate gradient relaxation. Structural optimizations were continued until the forces on the atoms had converged to less than 1 meV/Å and the pressure on the cell was minimized using stress minimization. The calculations were performed within periodic boundary conditions allowing the expansion of the crystal wave functions in terms of a plane-wave basis set.

The generalized gradient approximation (GGA) (Ref. 46) includes the effects of local gradients in the charge density for each point which generally gives better equilibrium structural parameters than the local-density approximation. A former study[6] confirms that the GGA is able to reproduce experimentally observed properties of BFO correctly. Thus, we have used GGA for all our studies. In the basis we treated explicitly 15 valence electrons for Bi ($5d^{10}6s^26p^3$), 11 for La ($5s^25p^65d^16s^2$), 14 for Fe ($3p^63d^64s^2$), 13 for Mn ($3p^63d^54s^2$), and 6 for oxygen ($2s^22p^4$). Brillouin-zone integrations are performed with a Gaussian broadening of 0.1 eV during all structural optimizations. These calculations are performed with a $4\times4\times4$ Monkhorst-Pack **k**-point mesh centered at the Γ point in the Brillouin zone. One specific problem of these materials is the presence of "computationally unfriendly" atom configurations such as the first-row element oxygen and the transition metal iron. Both are atoms which require extra care; either large basis sets within a pseudopotential scheme or an all-electron scheme. We chose to use a very large basis set with 700 eV for the plane-wave cutoff. The supercell approach was adopted to simulate the substitution of La/Mn in BFO and in all the calculations we have used collinear antiferromagnetic configurations. In order to simulate the experimental composition of $BiFe_{0.7}Mn_{0.3}O_3$ a supercell with composition $Bi_6Fe_4Mn_2O_{18}$ was constructed and for the $Bi_{0.9}La_{0.1}FeO_3$ case the close composition supercell of $Bi_5LaFe_6O_{18}$ was considered. The cations were substituted periodically and no disorder effects were considered in the calculations but proper antiferromagnetic ordering is considered.

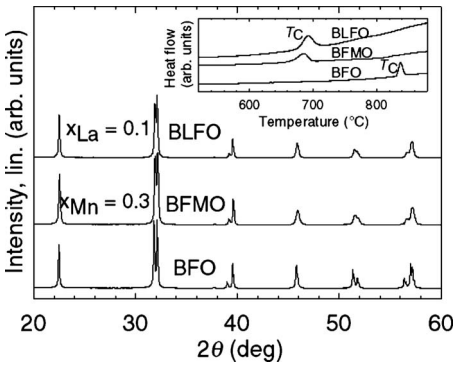

FIG. 1. XRD patterns of BFO, BFMO, and BLFO. Inset: DTA traces (endothermal up) depicting the ferroelectric Curie temperature T_C.

The RSMS algorithm FEFF (Ref. 42) has been used to calculate local symmetry-projected DOS and ELNES spectra with and without a core hole.[39] FEFF applies a self-consistent muffin-tin potential with Hedin-Lundquist self-energies to calculate scattering potentials, and automatically includes relativistic effects. Here, calculations were found to converge for clusters of 177 atoms. All spectra are simulated without a core hole, as this was found to give better experimental match than simulations with a core hole. In addition, an exchange potential of 2 eV has been applied to obtain the correct Fermi level, as it is shown[6] that magnetic exchange interactions are vital to a correct estimation of the Fermi level and thus insulating behavior of BFO. To enhance the differences between substituted and pure BFO, spectra have been simulated in which all Bi (Fe) atoms have been substituted with La (Mn) atoms. With FEFF, we are also able to calculate the local symmetry-projected DOS for BFO and the fully substituted structures.

III. RESULTS AND DISCUSSION

XRD patterns of the samples investigated in this paper are displayed in Fig. 1, showing that there are no peaks from residual secondary phases ($Bi_2Fe_4O_9$ and $Bi_{25}FeO_{39}$). The inset of Fig. 1 shows the ferroelectric Curie temperature T_C, determined from the onset of the endothermal peaks upon heating. The T_C of BFMO and BLFO is 150–160 °C lower than that of pure BFO, 825 °C. Table I gives the refined experimental and theoretical hexagonal lattice parameters (a_{hex}, c_{hex}), as well as experimental primitive unit-cell volume (V_{prim}), rhombohedral angle (α_{rh}), polar displacements of Bi/La (s) and Fe/Mn (t) relative to their centrosymmetric reference positions in a hypothetical $R\bar{3}c$ structure, and the ferroelectric Curie temperature (T_C) of BFO, BFMO, and BLFO.

The ELNES spectra of the O K edge of BFO (top), BFMO (middle), and BLFO (bottom) are shown in Fig. 2. The spectra are offset vertically for ease of comparison and

TABLE I. Calculated equilibrium hexagonal unit-cell parameters a_{hex} and c_{hex} for BFO, $BiFe_{2/3}Mn_{1/3}O_3$ and $Bi_{5/6}$ $La_{1/6}FeO_3$ obtained from stress and force minimization in VASP. Experimental crystallographic properties (hexagonal unit-cell parameters a_{hex} and c_{hex}, volume of primitive unit cell V_{prim}, rhombohedral angle α_{rh}, and displacement parameters s and t for Bi/La and Fe/Mn, respectively), and Curie temperatures T_C of BFO, BFMO, and BLFO. Note that the experimental and theoretical compositions of BFMO and BLFO differ slightly.

	DFT parameters		Experimental parameters						
Sample	a_{hex} (Å)	c_{hex} (Å)	a_{hex} (Å)	c_{hex} (Å)	V_{prim} (Å^3)	α_{rh} (°)	s (Å)	t (Å)	T_C (°C)
BFO	5.5697[a]	13.882[a]	5.579(2)	13.870(8)	62.32(1)	59.34(6)	0.73(3)	0.33(3)	825 ± 5
BFMO	5.5719	13.8113	5.574(9)	13.832(0)	62.05(1)	59.43(6)	0.64(6)	0.39(2)	666 ± 5
BLFO	5.5787	13.8067	5.579(4)	13.808(0)	62.04(1)	59.54(7)	0.60(0)	0.23(0)	675 ± 5

[a]Reference 6.

shifted horizontally to the same edge onset as no attempt has been made in this study to measure absolute edge onsets or chemical shifts. The experimental edges consist of two major peaks (labeled A and B in Fig. 2) and are in agreement with a previously published XANES study of BFO.[23]

A. BFO

In Fig. 3, we show the experimental as well as calculated O *K* edge of BFO and compare those with DOS calculations. It is interesting to note the similarity to the near-edge structure of α-Fe_2O_3,[47,48] which also contain FeO_6 octahedra with Fe in 3+ state. de Groot[49] interpreted the O *K* edge for transition metal oxides and attributed the first peak up to about 5 eV above E_F to transitions to energy states of mixed O *p* and TM *d* character, with a peak splitting characteristic of the crystal-field splitting in the material with low-energy t_{2g} π-bonding orbitals pointing between the O atoms and higher energy e_g σ-bonding orbitals to the O atoms. The second peak was attributed to states of mixed O *p* and TM *s* and *p* characters. It is now tempting because of the mainly ionic bonding in perovskites[50] and the similar edge shape, to assume that the Bi atoms form ionic bonds to O and thus have only minor influence on the O *K* edge shape, allowing us to directly apply the same bonding scheme as in the case of transition metal oxides. We will, however, on the basis of comparisons to density-of-states and RSMS calculations of

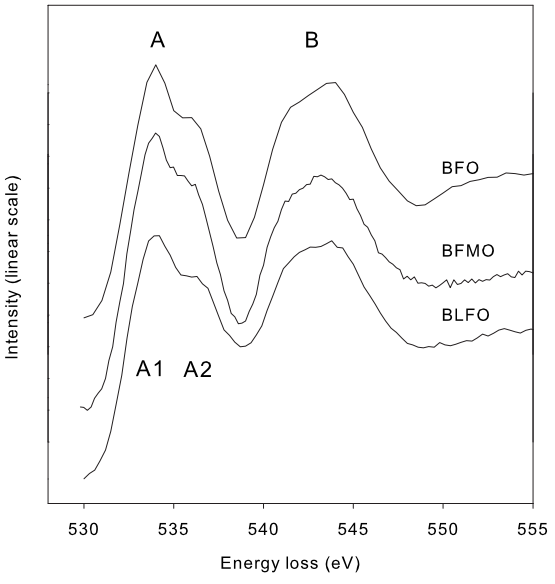

FIG. 2. Experimental background subtracted O *K* edge of $BiFeO_3$ (top), $BiFe_{0.7}Mn_{0.3}O_3$ (middle), and $Bi_{0.9}La_{0.1}FeO_3$ (bottom).

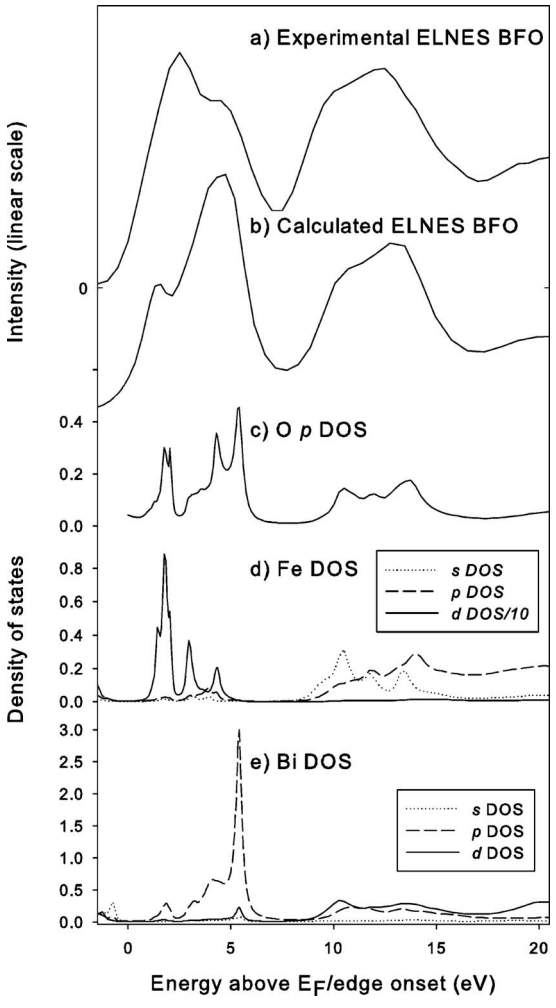

FIG. 3. (a) Experimental near-edge structure of BFO and (b) RSMS calculated near-edge structure of BFO. (c) O *p*, (d) Fe, and (e) Bi symmetry-projected unoccupied DOS of BFO from RSMS calculations. The Fe *d* DOS is scaled by a factor of 1/10.

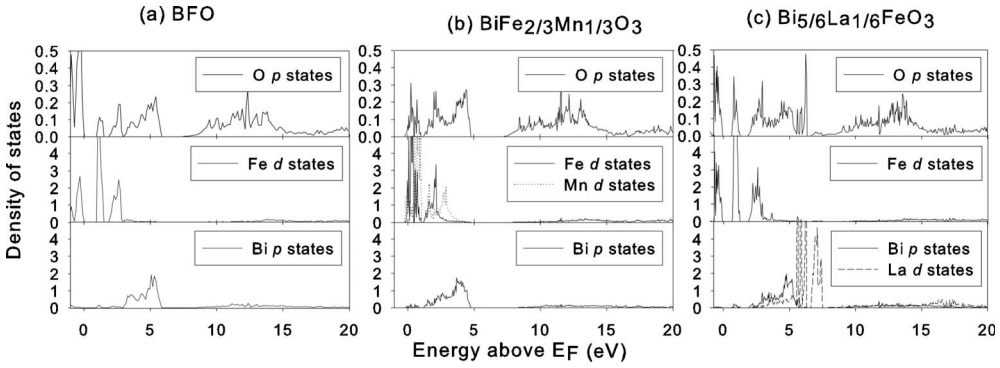

FIG. 4. O p (top), Fe d (middle), and Bi p (bottom) unoccupied DOS of (a) BFO, (b) $BiFe_{2/3}Mn_{1/3}O_3$, and (c) $Bi_{5/6}$ $La_{1/6}FeO_3$ from DFT calculations.

the fine structure, argue that the picture is less straightforward.

The RSMS O K edge is shown in Fig. 3(b). The overall shape of the edge in BFO and especially the peak positions are well reproduced, however the intensity at the edge onset (peak A1) is underestimated or some of the intensity is shifted in energy to coincide with peak A2. Although ELNES is not quantitatively comparable to DOS without knowledge of the energy-dependent matrix element or weighting factor, conclusions on bonding and electronic structure can still be drawn in a qualitative manner. The calculated partial DOS from the RSMS approach is shown in Figs. 3(c)–3(e). As a check of the reliability of this method, the same local DOS was also calculated by DFT, of which the most important states are shown in Fig. 4. The DOS from the two methods are generally found to be in good agreement, though the finite cluster size of the RSMS calculations introduces a smearing of the states. Also, the calculations differ in the energy area just above the Fermi level, where the RSMS approach fails to account correctly for the Fe d-band splitting. Despite these differences, there is a very good overall correspondence between the RSMS and DFT calculations. This overall good correspondence of the RSMS calculations is quite surprising in the case of BFO and similar compounds even with the use of a self-consistent potential, as the muffin-tin or spherically symmetric potential is not a good approximation for d electron orbitals or atoms with a lone pair of electrons, such as Bi. It has been suggested that although the directionality (and hence crystal-field splitting) of the d orbitals are not considered in the potential calculations, it still shows up in the scattering path calculations due to the geometrical anisotropy.[51]

The two main peaks A and B in Fig. 2 are easily recognized in the O p DOS, even if the intensity of peak A1 is not comparable to the intensity of the corresponding density of states. The origin of peak A1 is clear when comparing the O p and the Fe d states in Figs. 3(c) and 3(d), which form a covalent bond up to 3 eV above the edge onset. The crystal-field splitting of the 3d band into states of (in the idealized cubic perovskite structure situation) t_{2g} and e_g symmetries is visible in the Fe d states calculated by the RSMS method, however the relative intensity of the peaks and strength of the O p-Fe d bonding are different from the predictions of the DFT approach shown in Fig. 4.

Thus, we interpret the A1 and A2 peaks not as mainly due to the crystal-field splitting in BFO, as would be natural from the study of transition metal oxides.[49] The crystal-field splitting seems to be contained mainly within peak A1 and is not resolved experimentally in this work. This is in line with the XANES data on BFO of Park *et al.*,[23] where the splitting of the Fe L_2 and L_3 peaks are not resolved even with an energy resolution of 0.2 eV, and those of Higuchi,[24] who barely pick out a shoulder on the O K edge at an energy resolution of 0.2 eV. The results from RSMS calculations show that peak A2 can be explained by backscattering on O^{2-} ions while also having a contribution from covalent bonding to Bi states. It has been suggested earlier that the origin of this peak is Bi 5d states[23] and Bi sp states.[24] However, upon comparison to the Bi DOS in Fig. 3(e), we find that there are mainly Bi states of p character involved, although some Fe d states are also situated in this energy range. This shows that O p states do participate in bonding with Bi p states in BFO so that the bonding between O and Bi has a certain degree of covalent character. This has been predicted earlier by DFT calculations,[6] and this interpretation is in line with other perovskites such as $BiMnO_3$ (Ref. 51), $BaTiO_3$ (Ref. 52), and $PbTiO_3$ (Refs. 53 and 54), which also contain an A cation lone pair of electrons that is responsible for the ferroelectricity.[34] We note that our results differ from the calculations of Jan *et al.*[55] on various Pb- and Ti-based perovskites on the position of the peaks, they find that the t_{2g}-e_g splitting is large enough to surround the O p-B site p states. Although $PbTiO_3$ and BFO are in many ways similar, as Bi^{3+} and Pb^{2+} both have the same electron configuration and a lone pair of electrons, they differ in their B cation d band occupancy as Ti^{4+} is in d^0 state and Fe^{3+} is in high spin d^5 state. Thus, the ferroelectricity in $PbTiO_3$ has contribution from Ti-O bonds[54] while it has been suggested theoretically that the corresponding Fe-O bonding in BFO is less important.[6]

Peak B originates from scattering to an energy band 8–15 eV above the Fermi energy. The covalent oxygen-transition metal bond in this energy range is well known for both transition metal oxides[48,56] and perovskites,[49,57] and cluster calculations[57] have attributed this peak to predominantly backscattering from the O^{2-} ions. While confirming this interpretation by our RSMS calculation, we see from Fig. 3(e) that in BFO this energy range also has Fe s and p characters,

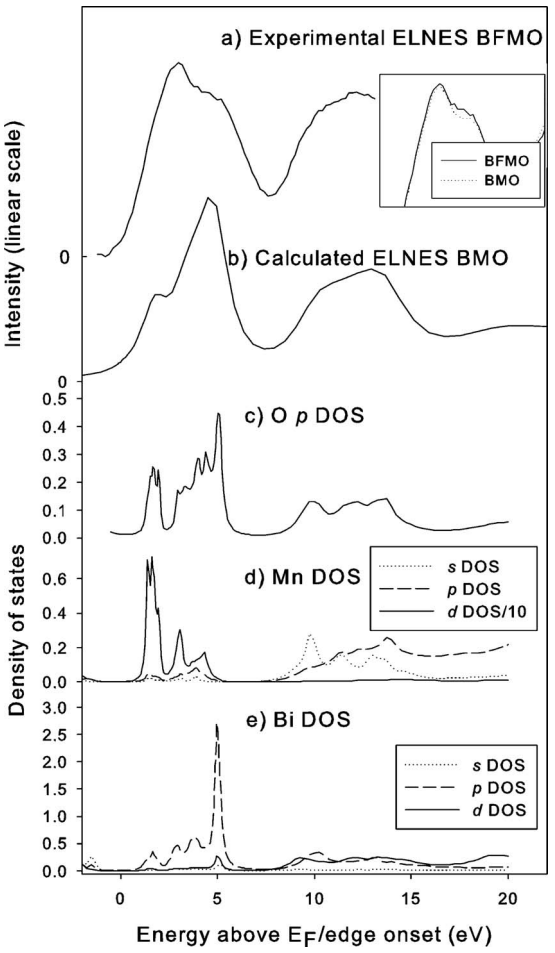

FIG. 5. (a) Experimental near-edge structure of BFMO and (b) RSMS calculated near-edge structure of fully substituted BMO. Inset to (a): comparison of the A peaks of BFMO (solid line) and BFO (dotted line). (c) O *p*, (d) Fe, and (e) Bi symmetry-projected unoccupied DOS of BMO from RSMS calculations. The Mn *d* DOS is scaled by a factor of 1/10.

and some contribution from covalent bonding to Bi states.

B. BFMO

The present total-energy calculations suggest that Mn is in 3+ oxidation state while the ground state of $BiFe_{2/3}Mn_{1/3}O_3$ is antiferromagnetic, in concordance with experimental results.[18,58] For computational simplicity we have considered only the simple collinear antiferromagnetic ordering found in BFO. As a result, the calculated total density of states for $BiFe_{2/3}Mn_{1/3}O_3$ [Fig. 4(b)] shows metallic behavior with a DOS at the Fermi level of 4 states eV^{-1} f.u.$^{-1}$. Underestimation of the band gap by DFT calculations is commonly observed. Conductivity measurements and spectroscopic studies show that BFO remains a semiconductor also when Fe is substituted with Mn.[17,59]

Figure 5(a) shows the experimental near-edge structure of BFMO. A comparison to the near-edge structure of BFO [inset of Fig. 5(a)] shows that upon substitution of Fe with Mn, the A2 peak is higher relative to the A1 peak. The higher A2 peak is in qualitative agreement with the RSMS calculations shown in Fig. 5(b), where we have simulated the situation for the fully substituted structure $BiMnO_3$ (BMO). We have chosen to simulate the fully substituted structure to emphasize the differences due to substitution while using the experimentally found structural parameters of BFMO. Also included in Fig. 5 are selected local densities of states for the fully substituted BMO. The higher intensity is easily interpreted as more empty states due to the one *d* electron less in Mn^{3+} compared to Fe^{3+}, and follows the general trend across the transition metals noted by de Groot[56] for transition-metal oxides. It is however at first sight surprising that the higher intensity is found in the A2 peak rather than the A1 peak, based on the assignment of A1 to Fe-O bonds and A2 to Bi-O bonds in BFO. Though the absolute intensities are difficult to measure experimentally, this interpretation is in agreement with the RSMS calculations of the two compounds, also showing that the increased intensity appears at A2 [Figs. 3(b) and 5(b)]. The DOS calculations of BMO shown in Figs. 4(b) and 5(c)–5(e) confirm that the same atomic orbitals are involved in bonding in BFMO as in BFO and that peak A2 is indeed a result of a covalent Bi-O bond also in BFMO. This Bi-O bond is shifted to lower energies than in BFO and shows that *B* site substitution affect the electronic structure also of the *A* site cation of BFO. We note that the XAS experiments of Higuchi[24] show that peak A2 (their peak *c*) is decreased by Mn substitution. They explain this by the oxygen vacancies in their sample and thereby a certain amount of Fe^{2+}, which could contribute to a higher A1 peak.[24]

According to recent studies,[14,36,60] the ferroelectric phase transition (Curie) temperature decreases with increasing Mn substitution. As was shown in Fig. 1, this was confirmed in our samples. Also, the atomic positions were found both experimentally and theoretically to approach the cubic perovskite structure and to adopt more homogeneous Bi-O bond lengths (Table I) and, of particular interest here, the displacement of the Bi ions decreases more with increasing Mn content than the displacement of Mn/Fe itself. Thus, it is clear that *B* site substitution also affects the *A* site cation. A similar connection is found theoretically in other Bi perovskites with varying *B* site cations,[61] where the O *p*-*B* site *d* bonding was found to affect the position of the O *p*-Bi *p* band. This implies that, although in the traditional picture the ferroelectricity is due to displacement of Bi ions, the importance of Fe on the ferroelectricity of the material should not be underestimated. We propose that this connection between Bi and Fe could exist through the small but important covalent part of the bonding of both Fe and Bi to O *p* states. This contributes to highlight the very complex interplay between charge transfer, degree of covalency, and ferroelectric properties in these materials.

C. BLFO

Upon substitution of La by Bi, an insulating behavior is maintained in the DFT calculations, giving a calculated band-gap value for $Bi_{5/6}La_{1/6}FeO_3$ of 0.66 eV. It may be noted that the band-gap value obtained from the present type of calculation will always be smaller than the corresponding

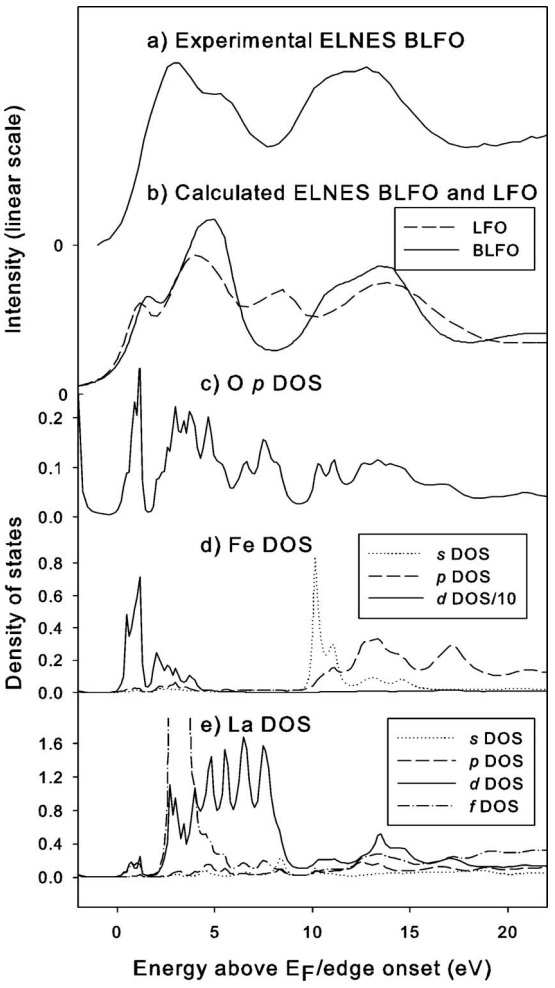

FIG. 6. (a) Experimental near-edge structure of BLFO and (b) RSMS calculated near-edge structure of fully substituted LFO (dashed line) and an approximation to BLFO (full line). (c) O *p*, (d) Fe, and (e) La symmetry-projected unoccupied DOS of LFO from RSMS calculations. The Fe *d* DOS is scaled by a factor of 1/10.

experimental value due to the well-known underestimation of band gap by DFT methods.

The experimental near-edge structure of BLFO and the RSMS calculated ELNES for the fully substituted $LaFeO_3$ (LFO) is shown in Fig. 6, together with selected local DOS of LFO. Though a crude approximation, we also include the weighted sum of the BFO and LFO spectra in order to see the effect of $x_{La}=0.1$, corresponding to the experimental data. In this approximation, and when comparing to local DOS of LFO, the assumption is implicitly made that the influence of La on the BLFO scales linearly with the amount of La, an assumption that at this stage cannot be verified. However, the correspondence to the experimental results indicate that at least to a first approximation, this may be a good way to explore the influence of La. Comparing the experimental near-edge structures of LFO and BFO (Fig. 2), it is clear that the changes upon adding La to the system are larger than substitution with Mn, even with a smaller degree of La substitution. The effect of La substitution on the near-edge structure seems to be a decrease in the overall intensity of the O *K* edge. This effect can be explained by considering the electronegativities of Bi and La: while the electronegativity of Bi is about 2 on the Pauling scale, La has a value of 1.1, only half the value of Bi. Thus, an increased number of electrons are expected on the Fe and O sites and hence less available DOS above E_F. A reduction in fine-structure features can therefore directly be related to a decrease in covalent bond strength, which is then directly linked to the differences in electronegativity of the involved atoms.

Looking at the relative intensities of the peaks, we see that the intensity ratio of peak A1 to peak B decrease while the intensity in the area between peaks A and B is clearly increased. Both of these features are qualitatively reproduced in the RSMS calculations. As in BFO, the A1 is due to bonding with Fe *d* states. The reduced intensity of this peak is in agreement with the ELNES study of Abbate *et al.*,[62] showing the O *K* edge of the other end member LFO with a higher A2 peak than A1. The decreased intensity in this part of the spectrum is also found in the Fe *d* DOS, showing a reduction in Fe *d* DOS for LFO compared to BFO. Again, we attribute this to the decreased electronegativity of La compared to Bi, giving less available DOS also on the Fe site.

According to the RSMS calculations, the intensity is reduced also for the A2 peak. In pure BFO and Mn-substituted BFMO, the A2 peak is partially explained by involving Bi *p* states. In La-substituted BLFO, the situation is slightly more complicated, though there is still a covalent contribution to the La-O bond. By comparison to the local DOS of fully substituted LFO from RSMS calculations [Figs. 6(c)–6(e)] and the partially substituted structure from DFT calculations [Fig. 4(c)], it is clear that the La-O bonding is not mediated through La *p* states but rather involves La states of *d* character that are located in sharp bands higher in energy than the Bi *p* states. These La *d* states are responsible for the increased intensity in the area between peaks A and B. The Bi *d* states are higher in energy than the La *d* states and thus do not form covalent bonds to O *p* states while the Bi *p* states, responsible for the A2 peak, are too low in energy to contribute to the intensity in this energy range. In the fully substituted LFO structure, this extra intensity will grow to a separate peak in the O *K* edge, however at the 10% experimental substitution level, the only recognizable feature is an increase in intensity between the A and B peaks. Hence, although more ionic, the bonding between La and O certainly has noticeable covalent character.

For the B peak, the O *p* states are shifted to higher energies in the fully substituted LFO structure; however this energy shift is not large enough to see experimentally in the 10% filled structure. Although the BLFO B peak shape has a quite similar appearance to pure BFO in both the experimental edge and the RSMS calculations, the Fe *s* states, responsible for part of the B peak in BFO, are in LFO located in a sharp band lower in energy than the relevant O *p* states and are seemingly not as involved in bonding as in BFO.

Though both La and Mn substitutions have been reported to improve the ferroelectric properties of BFO,[11,19,63] attempts to measure bulk single-crystalline, stoichiometric spontaneous polarization values are often hampered by leakage currents due to defects or impurities.[12,62,64] However, both the introduction of La on *A* site and Mn on *B* site have been found to lower the Curie temperature T_C (Fig. 1). As a

high T_C is often connected to high spontaneous polarization,[65] it is likely that the spontaneous polarization decreases in both cases. In BLFO, this is straightforwardly understood as La^{3+} does not have an ns^2 lone pair that according to DFT calculations[6] is responsible for 98% of the ferroelectricity in BFO. In the case of Mn substitution, the traditional picture of purely ionic *A* site-O bonding and no bond between the *A* and *B* sites is not sufficient to explain the lowering of T_C. The coupling could be mediated through small but still significant covalent bonds of O to both Fe/Mn and Bi. Also, though the overlap is small, Fe *d* states are also found in the area 2–4 eV above the edge onset of BFO, where also Bi *p* states are located (Fig. 4). In the same energy region, Ravindran[6] finds (by the crystal orbital Hamiltonian population method) a small but finite bonding between Fe and Bi. It is interesting that upon substitution with both Mn and La, this overlap increases so that the separation of O *p* states into bonding to Fe and La is less straightforward and should be looked into by methods also showing the spatial arrangement of bonds, e.g., by electron or x-ray diffraction techniques.[66]

Finally, we would like to comment on the magnetic properties of BFO. It has been shown experimentally that the polarization and magnetization is indeed coupled in BFO, in fact the coupling in bulk BFO where the magnetic ordering exhibits a (locally) antiferromagnetic structure with a long-range (~62 nm) cycloidal modulation was even found to be stronger than expected.[63] The microscopic origin of this coupling is not yet understood,[67] as the Bi^{3+} ions are responsible for (most of) the polarization while the Fe^{3+} ions are responsible for the magnetic properties. In other materials with a frustrated spin structure, the existence of polarization can be explained by the inverse Dzyaloshinskii-Moriya effect[68,69] by a shift of oxygen octahedra. In BFO, this is a weak contribution to the ferroelectricity which is mainly induced by a geometrical shift of Bi^{3+} ions.[6] Unlike BFO, the O *p*-*B d* and O *p*-Bi *p* band was not found to overlap for the nonmagnetic $BiBO_3$ compounds with *B*=Al, In, Ga, or Sc.[60] Hence, the coupling of Bi and Fe through covalent bonding to oxygen could play an important part also for the magnetoelectric coupling and further insight into the electronic structure could certainly aid the fundamental understanding of this phenomenon.

IV. CONCLUSIONS

Experimental and RSMS calculated near-edge structure of the O *K* edge of $BiFeO_3$, $Bi_{0.9}La_{0.1}FeO_3$, and $BiFe_{0.7}Mn_{0.3}O_3$ have been studied in detail and compared to RSMS calculations. The spectral features are explained by comparison to local DOS from RSMS and DFT calculations, and differences between the substituted and unsubstituted compounds have been interpreted in terms of bonding, charge transfer, and electronegativities. Specifically, it is confirmed that the bonding in $BiFeO_3$ has partial covalent character and that O atoms are covalently bound via O *p* states to both *A* and *B* site cations, providing a potentially important link between the *A* and *B* sites. Mn substitution on Fe sites is found to alter the electronic structure very little with the most important change actually happening on the Bi site through charge transfer and bonding effects, in agreement with the average structure from XRD.[36] Substitution of Bi with La leads to a larger alteration of the electronic structure, with the most notable differences being more ionic bond character and a covalent La-O bond being mediated through La *d* states rather than *p* states as the Bi-O bond. Thus, we show that there is a stronger connection between the *A* and *B* sites of $BiFeO_3$ than previously recognized, which at least in part could be explained by Fe-O and Bi-O covalent bonding.

*randi.holmestad@ntnu.no

[1] J. B. Neaton, C. Ederer, U. V. Waghmare, N. A. Spaldin, and K. M. Rabe, Phys. Rev. B **71**, 014113 (2005).
[2] Y. P. Wang, L. Zhou, M. F. Zhang, X. Y. Chen, J.-M. Liu, and Z. G. Liu, Appl. Phys. Lett. **84**, 1731 (2004).
[3] T. Zhao, A. Scholl, F. Zavaliche, K. Lee, M. Barry, A. Doran, M. P. Cruz, Y. H. Chu, C. Ederer, N. A. Spaldin, R. R. Das, D. M. Kim, S. H. Baek, C. B. Eom, and R. Ramesh, Nature Mater. **5**, 823 (2006).
[4] G. Catalan and J. F. Scott, Adv. Mater. **21**, 2463 (2009).
[5] F. Kubel and H. Schmid, Acta Crystallogr., Sect. B: Struct. Sci. **46**, 698 (1990).
[6] P. Ravindran, R. Vidya, A. Kjekshus, and H. Fjellvåg, Phys. Rev. B **74**, 224412 (2006).
[7] X. Qi, J. Dho, R. Tomov, M. G. Blamire, and J. L. MacManus-Driscoll, Appl. Phys. Lett. **86**, 062903 (2005).
[8] V. A. Khomchenko, D. A. Kiselev, J. M. Vieira, A. L. Kholkin, M. A. Sá, and Y. G. Pogorelov, Appl. Phys. Lett. **90**, 242901 (2007).
[9] Y. Wang and C.-W. Nan, Appl. Phys. Lett. **89**, 052903 (2006).
[10] S.-T. Zhang, L.-H. Pang, Y. Zhang, M.-H. Lu, and Y.-F. Chen, J. Appl. Phys. **100**, 114108 (2006).
[11] Z. X. Cheng, A. H. Li, X. L. Wang, S. X. Dou, K. Ozawa, H. Kimura, S. J. Zhang, and T. R. Shrout, J. Appl. Phys. **103**, 07E507 (2008).
[12] S. R. Das, R. N. P. Choudhary, P. Bhattacharya, R. S. Katiyar, P. Dutta, A. Manivannan, and M. S. Seehra, J. Appl. Phys. **101**, 034104 (2007); S. R. Das, P. Bhattacharya, R. N. P. Choudhary, and R. S. Katiyar, *ibid.* **99**, 066107 (2006).
[13] G. Le Bras, D. Colson, A. Forget, N. Genand-Riondet, R. Tourbot, and P. Bonville, Phys. Rev. B **80**, 134417 (2009).
[14] J. R. Sahu and C. N. R. Rao, Solid State Sci. **9**, 950 (2007).
[15] V. R. Palkar, D. C. Kundaliya, and S. K. Malik, J. Appl. Phys. **93**, 4337 (2003).
[16] S. M. Selbach, M.-A. Einarsrud, and T. Grande, Chem. Mater. **21**, 169 (2009).
[17] S. M. Selbach, T. Tybell, M.-A. Einarsrud, and T. Grande, Phys. Rev. B **79**, 214113 (2009).
[18] I. Sosnowska, W. Schafer, W. Kockelmann, K. H. Andersen, and I. O. Troyanchuk, Appl. Phys. A: Mater. Sci. Process. **74**, s1040

(2002).
[19] Q.-H. Jiang, C.-W. Nan, and Z.-J. Shen, J. Am. Ceram. Soc. **89**, 156 (2006).
[20] Z. Zhang, P. Wu, L. Chen, and J. Wang, Appl. Phys. Lett. **96**, 012905 (2010).
[21] J. R. Chen, W. L. Wang, J. B. Lia, and G. H. Rao, J. Alloys Compd. **459**, 66 (2008).
[22] S. Karimi, I. M. Reaney, Y. Han, J. Pokorny, and I. Sterianou, J. Mater. Sci. **44**, 5102 (2009).
[23] T.-J. Park, S. Sambasivan, D. A. Fischer, W.-S. Yoon, J. A. Misewich, and S. S. Wong, J. Phys. Chem. C **112**, 10359 (2008).
[24] T. Higuchi, Y.-S. Liu, P. Yao, P.-A. Glans, J. Guo, C. Chang, Z. Wu, W. Sakamoto, N. Itoh, T. Shimura, T. Yogo, and T. Hattori, Phys. Rev. B **78**, 085106 (2008).
[25] J. A. McLeod, Z. V. Pchelkina, L. D. Finkelstein, E. Z. Kurmaev, R. G. Wilkis, A. Moeves, I. V. Solovyev, A. A. Belik, and E. Takayama-Muromachi, Phys. Rev. B **81**, 144103 (2010).
[26] S. H. Xie, J. Y. Li, R. Proksch, Y. M. Liu, Y. C. Zhou, Y. Y. Liu, Y. Ou, L. N. Lan, and Y. Qiao, Appl. Phys. Lett. **93**, 222904 (2008).
[27] S. H. Basu, M. Pal, and D. Chakravorty, J. Magn. Magn. Mater. **320**, 3361 (2008).
[28] T.-J. Park, G. C. Papaefthymiou, A. J. Viescas, A. R. Moodenbaugh, and S. S. Wong, Nano Lett. **7**, 766 (2007).
[29] X. Qi, M. Wei, Y. Lin, Q. Jia, D. Zhi, J. Dho, M. G. Blamire, and J. L. MacManus-Driscoll, Appl. Phys. Lett. **86**, 071913 (2005).
[30] Y. B. Chen, M. B. Katz, X. Q. Pan, R. R. Das, D. M. Kim, S. H. Baek, and C. B. Eom, Appl. Phys. Lett. **90**, 072907 (2007).
[31] F. Tyholdt, H. Fjellvåg, A. E. Gunnæs, and A. Olsen, J. Appl. Phys. **102**, 074108 (2007).
[32] J. Wang, H. Zheng, Z. Ma, S. Prasertchoung, M. Wuttig, R. Droopad, J. Yu, K. Eisenbeiser, and R. Ramesh, Appl. Phys. Lett. **85**, 2574 (2004).
[33] R. R. Das, D. M. Kim, S. H. Baek, C. B. Eom, F. Zavaliche, S. Y. Yang, R. Ramesh, Y. B. Chen, X. Q. Pan, X. Ke, M. S. Rzchowski, and S. K. Streiffer, Appl. Phys. Lett. **88**, 242904 (2006).
[34] R. E. Cohen, Nature (London) **358**, 136 (1992).
[35] Y. Kuroiwa, S. Aoyagi, A. Sawada, J. Harada, E. Nishibori, M. Takata, and M. Sakata, Phys. Rev. Lett. **87**, 217601 (2001).
[36] S. M. Selbach, T. Tybell, M.-A. Einarsrud, and T. Grande, Chem. Mater. **21**, 5176 (2009).
[37] R. F. Egerton, *Electron Energy-Loss Spectroscopy in the Electron Microscope* (Plenum Press, New York, 1996).
[38] V. J. Keast, A. J. Scott, R. Brydson, D. B. Williams, and J. Bruley, J. Microsc. **203**, 135 (2001).
[39] K. van Benthem, C. Elsässer, and M. Rühle, Ultramicroscopy **96**, 509 (2003).
[40] E. J. Kirkland, Ultramicroscopy **102**, 199 (2005).
[41] J. J. Rehr and A. L. Ankudinov, Coord. Chem. Rev. **249**, 131 (2005).
[42] M. S. Moreno, K. Jorissen, and J. J. Rehr, Micron **38**, 1 (2007).
[43] P. E. Blöchl, Phys. Rev. B **50**, 17953 (1994).
[44] G. Kresse and J. Hafner, Phys. Rev. B **47**, 558 (1993); G. Kresse and J. Furthmuller, Comput. Mater. Sci. **6**, 15 (1996).
[45] G. Kresse and D. Joubert, Phys. Rev. B **59**, 1758 (1999).
[46] J. P. Perdew, in *Electronic Structure of Solids*, edited by P. Ziesche and H. Eschrig (Akademie Verlag, Berlin, 1991); J. P. Perdew, K. Burke, and Y. Wang, Phys. Rev. B **54**, 16533 (1996); J. P. Perdew, K. Burke, and M. Ernzerhof, Phys. Rev. Lett. **77**, 3865 (1996).
[47] C. Colliex, T. Manoubi, and C. Ortiz, Phys. Rev. B **44**, 11402 (1991).
[48] Z. Y. Wu, S. Gota, F. Jollet, M. Pollak, M. Gautier-Soyer, and C. R. Natoli, Phys. Rev. B **55**, 2570 (1997).
[49] F. M. F. de Groot, J. Faber, J. J. M. Michiels, M. T. Czyżyk, M. Abbate, and J. C. Fuggle, Phys. Rev. B **48**, 2074 (1993).
[50] T. Wolfram and S. Ellialtioglu, *Electronic and Optical Properties of d-Band Perovskites* (Cambridge University Press, Cambridge, 2006).
[51] H. O. Moltaji, J. P. Buban, J. A. Zaborac, and N. D. Browning, Micron **31**, 381 (2000).
[52] R. Seshadri and N. A. Hill, Chem. Mater. **13**, 2892 (2001).
[53] J. Zhang, A. Visinoiu, F. Heyroth, F. Syrowatka, M. Alexe, D. Hesse, and H. S. Leipner, Phys. Rev. B **71**, 064108 (2005).
[54] H. Miyazawa, F. Ishii, E. N. T. Shimoda, and T. Oguchi, Ferroelectrics **301**, 49 (2004).
[55] J. C. Jan, H. M. Tsai, C. W. Pao, J. W. Chiou, K. Asokan, K. P. Krishna Kumar, W. F. Pong, Y. H. Tang, M.-H. Tsai, S. Y. Kuo, and W. F. Hsieh, Appl. Phys. Lett. **87**, 012103 (2005); J. C. Jan, K. P. Krishna Kumar, J. W. Chiou, M.-H. Tsai, H. L. Shih, H. C. Hsueh, S. C. Ray, K. Asokan, W. F. Pong, H. M. Tsai, S. Y. Kuo, and W. F. Hsieh, *ibid.* **83**, 3311 (2003).
[56] F. M. F. de Groot, M. Grioni, J. C. Fuggle, J. Ghijsen, G. A. Sawatzky, and H. Petersen, Phys. Rev. B **40**, 5715 (1989).
[57] N. D. Browning, H. O. Moltaji, and J. P. Buban, Phys. Rev. B **58**, 8289 (1998).
[58] X. Yu and A. An, Solid State Commun. **149**, 711 (2009).
[59] T. Higuchi, T. Hattori, W. Sakamoto, N. Itoh, T. Shimura, T. Yogo, P. Yao, P. A. Glans, C. L. Chang, Z. Y. Wu, and J. H. Guo, Jpn. J. Appl. Phys. **47**, 7570 (2008).
[60] M. Azuma, H. Kanda, A. A. Belik, Y. Shimakawa, and M. Takano, J. Magn. Magn. Mater. **310**, 1177 (2007).
[61] H. Wang, B. Wang, Q. Li, Z. Zhu, R. Wang, and C. H. Woo, Phys. Rev. B **75**, 245209 (2007).
[62] M. Abbate, F. M. F. de Groot, and J. C. Fuggle, Phys. Rev. B **46**, 4511 (1992).
[63] M. Kumar and K. L. Yadav, Appl. Phys. Lett. **91**, 242901 (2007).
[64] D. Lebeugle, D. Colson, A. Forget, M. Viret, A. M. Bataille, and A. Gukasov, Phys. Rev. Lett. **100**, 227602 (2008).
[65] S. C. Abrahams, S. K. Kurtz, and P. B. Jamieson, Phys. Rev. **172**, 551 (1968).
[66] J. M. Zuo, M. Kim, M. O'Keeffe, and J. C. H. Spence, Nature (London) **401**, 49 (1999).
[67] K. F. Wang, J.-M. Liu, and Z. F. Ren, Adv. Phys. **58**, 321 (2009).
[68] I. A. Sergienko and E. Dagotto, Phys. Rev. B **73**, 094434 (2006).
[69] H. Katsura, N. Nagaosa, and A. V. Balatsky, Phys. Rev. Lett. **95**, 057205 (2005).